ROYAL SOCIETY OF CHEMISTRY

EDGE ARTICLE

Check for updates

Tailoring polymer-metal–organic frameworks (polyMOFs) using telechelic poly(octenamer)s

Prantik Mondal, [ID] Debobroto Sensharma [ID] and Seth M. Cohen [ID] *

Polymer-metal–organic frameworks (polyMOFs) represent an unusual class of polymer-MOF hybrids, but inadequate methods for designing and tailoring their underlying polymeric building blocks have been a limitation of these systems. Previous efforts in designing polyMOFs using random copoly(pentenamer)s resulted in a rather limited loading (30%) of benzene-1,4-dicarboxylic acid (H_2bdc; a.k.a, terephthalic acid) derived monomers into the polymer ligand. In this context, this study employs poly(octenamer)s that allowed for 100% incorporation of H_2bdc containing monomers. This was achieved by homopolymerising a new H_2bdc-tagged cyclooctene derivative through a controlled olefin-metathesis polymerisation in the presence of acyclic olefins as chain-transfer agents (CTAs). Using a novel CTA led us to achieve a homopolymer with reversible addition fragmentation chain-transfer (RAFT) telechelics, which was then utilized as a macroinitiator to polymerise styrene and produce ABA-type triblock copolymers, wherein a poly(octenamer) block was centered between two polystyrene (PS) blocks. Combining these polymers with Zn(II) produced polyMOFs with tunable structural morphologies influenced by the architecture, composition, and monomer content of the polymer ligand. Interestingly, the discrete thermoplastic PS domains enabled the corresponding crystalline polyMOFs to exhibit reversible glassy-to-rubbery characteristics at >100 °C.

Introduction

Metal–organic frameworks (MOFs) constitute a class of highly crystalline, porous solids composed of multi-topic organic ligands interconnected by inorganic secondary building units (SBUs).[1] The synergistic combination of (micro)crystalline, powdery MOFs with organic polymers can result in novel composite materials exhibiting unique properties and enhanced performance across a diverse range of applications.[2,3] Polymer-metal–organic frameworks (polyMOFs, Fig. 1) represent one class of polymer-MOF hybrids that are assembled through a bottom-up approach, whereby the organic component of the MOF is a polymer that possesses metal binding ligands capable of forming a MOF-like lattice.[4–8]

Engineering MOFs with controllable and tunable bulk characteristics, including tunable structural morphologies and thermal behavior, holds the potential to impart significant value-added characteristics to these crystalline materials and their corresponding composites.[9,10] Modulating such characteristics helps tune their functional properties across various domains, including catalysis, sorption, separation, sensing, and others.[11,12] The structural morphology of MOFs is primarily tuned through the control of external factors such as pH, temperature, modulators, or surfactants.[13] Glass transition in

MOFs represents another emerging thermal property that facilitates their reversible transformation into network-forming liquids or glasses.[14] This feature offers a straightforward fabrication method to transform a crystalline MOF to glassy monoliths, films, or membranes with potential applications in optics, separation, and other fields.[15,16] Nevertheless, the advancement of accessible methods for synthesizing MOFs with tailor-made bulk properties has presented a significant challenge, and examples of MOFs exhibiting such characteristics are rather limited.[9]

The incorporation of polymeric linkers, as an integral component of the polyMOF building unit, presents an opportunity to modulate and control the crystallinity, thermal stability, and structural morphology of polyMOFs.[3,6] The polymeric linkers simultaneously serve as the source of multitopic ligands for MOF formation and the architect of the MOF crystal structure. Using polymeric linkers enables tailoring the morphology of the corresponding polyMOFs *via* straightforward adjustments in their molar masses, dispersity, composition, and microstructures, a capability that is not readily accessible in parent MOFs constructed from molecular building blocks. This can be accomplished by exploiting the structural design of tailor-made polymeric struts, such as di- or tri-block copolymers, which consist of distinct polymeric blocks with benzene-1,4-dicarboxylic acid (H_2bdc; a.k.a., terephthalic acid) repeating units for MOF formation.

Department of Chemistry and Biochemistry, University of California, La Jolla, San Diego, California 92093, USA. E-mail: scohen@ucsd.edu
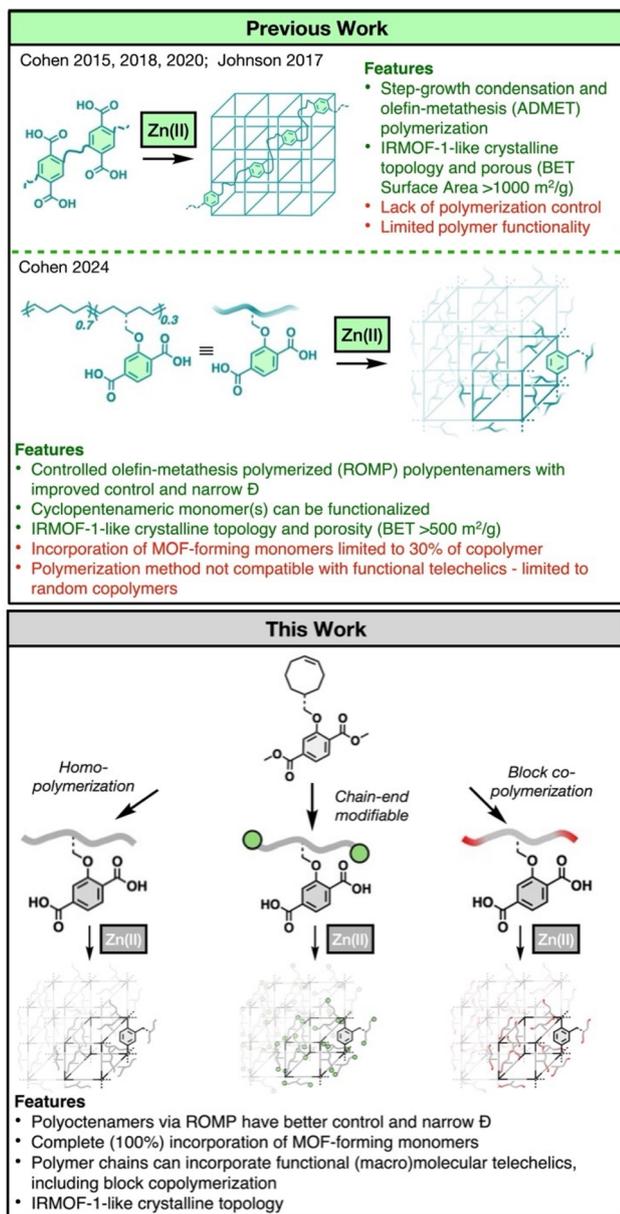
Fig. 1 (Top) Overview of polymer ligands developed by Cohen[18,19,23] and Johnson,[17] which incorporate ligating units either in their backbone or as pendant groups. Advantages (green) and disadvantages (red) are listed for each system. (Bottom) Use of a cyclooctene-tagged monomer enables the synthesis of customised telechelic homo- and block copoly(octenamer)s, which are subsequently converted into polyMOFs.

The reports of Johnson[17] and Cohen[18,19] describe the design of appending discrete polymeric blocks with oligo- or polymeric linkers containing H_2bdc units in their backbone and their utilization to assemble polyMOFs with controlled morphologies. Of particular note is the work of Ayala *et al.*,[18] which reported polyMOFs with an IRMOF-1 structure type using block copolymers that contain a distinct block of polymeric linker with H_2bdc repeating units in the main chain (referred to as 'pbdc'). The block copolymeric linkers were prepared in the

form of AB-diblock and ABA triblock copolymers, where pbdc and poly(ethylene glycol) (PEG) served as the A and B blocks, respectively. Notably, the polyMOFs derived from homopolymer analogues of pbdc crystallized into irregularly sized microcrystalline cubes, whereas the block copolymer analogues produced polyMOFs with uniform cubic morphology and size of ~1.8 μm. Interestingly, the dimensions of the polyMOFs decreased (~300–500 nm) while preserving their uniform cubic morphology as the percentage of PEG blocks increased.

In addition, the incorporation of a polymeric linker as the ligand strut should allow the resulting polyMOFs to inherit the thermal characteristics, such as glass transition or melting, of the polymer linker. Examples of MOFs that exhibit accessible glass transition and/or melting characteristics are primarily based on variants of zeolitic imidazolate framework (ZIF) structure type.[20,21] A controlled polymerization method could facilitate the engineering of a block copolymer linker consisting of a non-coordinating, amorphous polymeric block distinct from the polyMOF-forming block, where the amorphous domain would enable the vitrification of the corresponding polyMOF.

Macromolecular ligands containing H_2bdc units in their backbone are typically synthesised through step-growth, iterative, or acyclic diene metathesis polymerisation. Such approaches generally limit control over polymerisation, producing widely dispersed polymers, with lower molar masses, and limited opportunities for postpolymerisation modification. Due to a dearth of suitable monomers and controlled polymerisation methods, designing polyMOFs using tailor-made homopolymeric or block copolymeric linkers with dangling (*i.e.*, pendant) ligating units has had limited success.[5,22] Indeed, monomers with H_2bdc pendant groups would allow harnessing the advantages of diverse chain polymerisation methods, accessing emergent characteristics in the resultant polyMOFs. Recently, Cohen and coworkers employed a ring-opening metathesis polymerisation (ROMP) to synthesise poly(pentenamer)s with a controlled composition (30%) of H_2bdc pendants, which were subsequently converted into polyMOFs with structures resembling the canonical isoreticular MOF (IRMOF) type (Fig. 1).[23]

Telechelic polymers hold significant industrial importance due to their high propensity for postpolymerisation modifications, where "telechelic" refers to a polymer chain that is end-capped with useful chemical functionalities.[24] A prominent example of this is the extensive utilisation of telechelic poly(butadiene)s in the rubber and polyurethane industries as cross-linkers to produce sealants, adhesives, propellants, *etc.*[25,26] One of the most distinctive characteristics of telechelic polymers is their capacity to function as potent precursors to fabricate (multi)block copolymers. An ideal linear telechelic polymer should possess an average chain-end functionality ($\bar{F}_n$) of 2 per chain, as deviations from this value do not allow for formation of complete blocks and can diminish the overall performance of the resulting materials.[27]

(*Z*)-Cyclooct-4-ene derivatives are among the most extensively utilised strained cyclic olefins and can be readily polymerised using ROMP to produce robust, functional

poly(octenamer)s.[28,29] Applying acyclic olefins as chain transfer agents (CTAs) further enables the synthesis of ROMP-derived poly(octenamer)s with remarkably precise mass and composition control.[30,31] Symmetric CTAs are commonly employed to synthesize polyolefins with telechelics, resulting in polymer chains that possess identical chemical functionalities at both chain ends. The robustness and reliability of Grubbs' catalyst, coupled with the utilisation of appropriate CTA, can be leveraged to generate controlled poly(octenamer)s with $\bar{F}_n$ of approximately 2 per chain.

Herein, a cyclooctene-derived functional monomer was synthesised, polymerized *via* a CTA-mediated ROMP method, and hydrolysed to yield homopolymers with 100% H$_2$bdc dangling pendants (Fig. 1). Employing appropriate, symmetrical CTAs yielded telechelic homopolymers with functional groups at the chain termini ($\bar{F}_n$ ~2.0), including pentafluorophenyl esters or reversible addition–fragmentation chain transfer (RAFT) groups. These allowed the homopolymers to be modified postpolymerization by amine-containing molecules or further elaborated through RAFT polymerization to produce thermoplastic PS blocks. Combining such functional homo- and block copolymers with Zn(II) yielded polyMOFs with an IRMOF-1 structure type as evidenced by powder X-ray diffraction (PXRD), N$_2$ gas sorption, and Brunauer–Emmett–Teller (BET) surface area measurements. The ABA-type triblock copolymeric ligands enabled the corresponding polyMOFs to exhibit substantial structural morphology differences compared to polyMOFs based on homopolymer ligands. Moreover, this controlled polymerisation method facilitated the design of block copolymer linkers with a different fraction of PS blocks, which also exhibit a notable impact on modulating the structural morphology of the corresponding polyMOFs. Notably, the presence of non-coordinating, distinct PS blocks endowed the corresponding polyMOFs with characteristic glass transition behaviour at approximately 105 °C, as gauged by differential scanning calorimetry (DSC) and PXRD analyses. To the best of our knowledge, there have been no reports demonstrating polyMOFs based on telechelic homo- and block copolymeric linkers composing H$_2$bdc pendants, resulting in their unique structural and physical properties.

Results and discussion

Polymer synthesis and characterisation

Adapting an earlier synthetic protocol, dimethyl (*Z*)-2-(2-(cyclooct-4-en-1-yloxy)ethoxy)terephthalate, OCTbdc-5e (where "OCT" = cyclooctene; "e" = the methyl ester form of H$_2$bdc; "5" = the number of methylene units and oxygen atoms between the OCT unit and H$_2$bdc-ester moiety) was synthesised from (*Z*)-cyclooct-4-enol (Fig. S1 and S2). To perform the polymerisation, 0.2 equiv of Grubbs' second-generation (G2) catalyst was combined with a mixture of 24 equiv of OCTbdc-5e and 1 equiv of *n*-hexene as an "asymmetric" CTA at 30 °C for 18 h (Fig. 2).[32] After isolating the polymer product as a pale brown, sticky solid, the ester-protected polymer (poly(OCTbdc-5e)$_{35}$) was hydrolysed to obtain the desired homopolymeric linker, poly(OCTbdc-5a)$_{35}$ (where "a" refers to the acid form of H$_2$bdc and "35" refers to the number of repeating units). The chemical structure of the polymer was elucidated through ^{1}H NMR spectroscopy, revealing the emergence of distinctive proton signals indicative of OCTbdc-5e repeating units, with no discernible traces of residual monomer (Fig. S3). Size-exclusion chromatography (SEC) analysis of poly(OCTbdc-5e$_{35}$) provided a number-average molecular weight ($M_{n,\text{SEC}}$) value of 12.9 kDa ($Đ$ = 2.18), which closely corresponds to its $M_{n,\text{Theo}}$ value (8.7 kDa) (Fig. S4, and Table S1). Dividing the $M_{n,\text{SEC}}$ value by the molecular weight of OCTbdc-5e gave the degree of polymerisation (~35 repeat units).
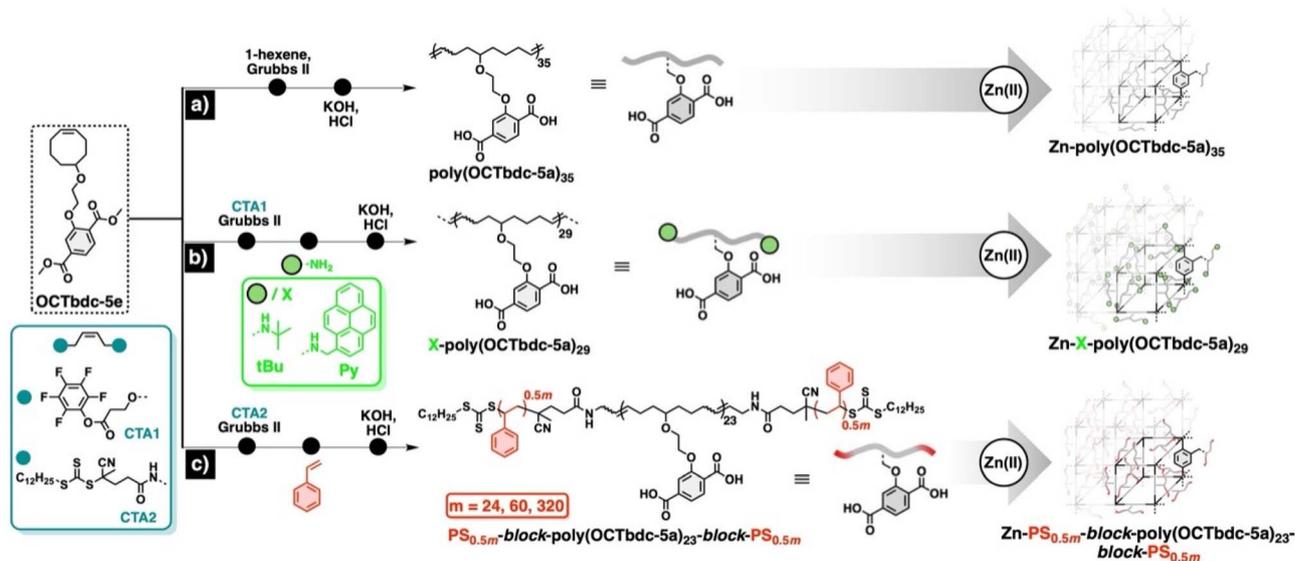

Fig. 2 Scheme for the synthesis of: (a) poly(OCTbdc-5a)$_{35}$, (b) X-poly(OCTbdc-5a)$_{29}$, and (c) PS$_{0.5m}$-*block*-poly(OCTbdc-5a)$_{23}$-*block*-PS$_{0.5m}$, followed by their combination with Zn(II) to yield Zn-poly(OCTbdc-5a)$_{35}$, Zn-X-poly(OCTbdc-5a)$_{29}$, and Zn-PS$_{0.5m}$-*block*-poly(OCTbdc-5a)$_{23}$-*block*-PS$_{0.5m}$.

To obtain a similar polymer ligand, but one amenable to postpolymerisation functionalization, a pentafluorophenol ester-terminated symmetric CTA (CTA1) was synthesised (Fig. S5)[33] and employed to obtain CTA1-poly(OCTbdc-5e)$_{29}$, wherein all polymer chains are anticipated to be capped with CTA1 at both their termini. ^{1}H and ^{19}F NMR spectroscopy of CTA1-poly(OCTbdc-5e)$_{29}$ showed characteristic terminal methylene and fluorine resonances of CTA1 moiety (Fig. S6).

The relative peak integration of the terminal protons to the polymer backbone signals yielded the $M_{n,\text{NMR}}$ (11.8 kDa) for CTA1-poly(OCTbdc-5e)$_{29}$, consistent with its $M_{n,\text{SEC}}$ (11.2 kDa). The relatively narrow dispersity ($Đ = 1.45$) of the polymer chains suggests that the symmetric CTA-mediated ROMP was controlled. If all the chains were ideally end-capped at both ends, the degree of polymerisation (per chain) should be 24-mers, with a $M_{n,\text{Theo}}$ of 9.3 kDa and $\bar{F}_n$ of 2 per chain.[34] Based on the degree of polymerisation obtained from ^{1}H NMR (~31-mers) or SEC (~29-mers), $\bar{F}_n$ is calculated to be ~1.65, indicating that a major proportion of the polymer chains (~83%) was telechelically end-capped with CTA1.

To illustrate its practical utility for end-capping polymer chains with a wide range of chemical functionalities, CTA1-poly(OCTbdc-5e)$_{29}$ was treated with amines, including *tert*-butylamine (*t*Bu) and pyren-1-yl methanamine (Py). The disappearance of the terminal proton and fluorine signals of CTA1 in the corresponding ^{1}H and ^{19}F NMR spectra (Fig. S7–S10) indicated the quantitative coupling of CTA1-poly(OCTbdc-5e)$_{29}$ with these amines. The functionalized polymers were designated as X-poly(OCTbdc-5e)$_{29}$, where "X" represents either *t*Bu or Py.

To expand the repertoire of polymeric linkers suitable for polyMOF formation, a coupling reaction with a polyether monoamine, Jeffamine M-2070, was performed to obtain ABA-type triblock copolymers. Regrettably, this approach did not yield complete conversion, as evidenced by residual CTA1 resonances in the ^{1}H and ^{19}F NMR spectroscopy of Jeff-1-poly(OCTbdc-5e)$_{29}$; however, the appearance of characteristic methyl signals of Jeffamine was observed in the reaction product (Fig. S11–S12). The $M_{n,\text{SEC}}$ value (12.5 kDa, $Đ = 1.45$) of Jeffamine-modified poly(OCTbdc-5e)$_{29}$ was slightly increased compared to CTA1-poly(OCTbdc-5e)$_{29}$ ($M_{n,\text{SEC}}$ (11.2 kDa)) and did not correlate with the expected $M_{n,\text{Theo}}$ value (15.2 kDa) that would be expected if all CTA1 groups were replaced with Jeffamine chains (Fig. S4).

Based on the failure of the Jeffamine amide coupling, another symmetric CTA (CTA2, Fig. S13 and S14) was designed and synthesised *via* a multi-step synthetic procedure (complete details are provided in the SI), which includes RAFT groups at both ends. A combination of CTA2, G2 catalyst, and OCTbdc-5e in toluene at 30 °C yielded CTA2-poly(OCTbdc-5e)$_{23}$, with $M_{n,\text{SEC}}$ (9.18 kDa, $Đ = 1.36$) and $M_{n,\text{NMR}}$ (8.83 kDa) values closely aligning with its $M_{n,\text{Theo}}$ (9.55 kDa) confirming the successful and well-controlled polymerisation process (Fig. S15, and Table S1). More significantly, based on the experimental degree of polymerisation (23-mers), $\bar{F}_n$ was determined to be ~2.0, indicating that >99% polymer chains were telechelically capped with RAFT functional groups.

CTA2-poly(OCTbdc-5e)$_{23}$ was employed as a macroinitiator to bulk polymerise 600 equiv. of styrene at 110 °C to produce a series of ABA-type triblock copolymers.[35] PS blocks were present at both ends of the polymer chain, while poly(OCTbdc-5e)$_{23}$ served as the middle block. The length of the PS blocks was modified by adjusting the duration of polymerisation reaction. Polymerisation times of 20 min, 120 min, and 840 min resulted in PS blocks with degrees of polymerisation of 24, 60, and 320, respectively. SEC analysis of all the triblock copolymers, designated as PS$_{0.5m}$-*block*-poly(OCTbdc-5e)$_{23}$-*block*-PS$_{0.5m}$ (where "*m*" represents the total degree of polymerisation of PS that is presumed to be evenly distributed between the two terminal blocks), unveiled a diminution in elution volumes, which is in accord with an increase in their corresponding molar masses compared to CTA2-poly(OCTbdc-5e)$_{23}$ (Fig. S16, S17 and Table S1).

As with poly(OCTbdc-5a$_{35}$), the other prepared poly(octenamer)s, namely *t*Bu-poly(OCTbdc-5e)$_{29}$, Py-poly(OCTbdc-5e)$_{29}$, and PS$_{0.5m}$-*block*-poly(OCTbdc-5e)$_{23}$-*block*-PS$_{0.5m}$, were hydrolysed to obtain *t*Bu-poly(OCTbdc-5a)$_{29}$, Py-poly(OCTbdc-5a)$_{29}$, and PS$_{0.5m}$-*block*-poly(OCTbdc-5a)$_{23}$-*block*-PS$_{0.5m}$, respectively, for their conversion to polyMOFs (Fig. S18).

PolyMOF synthesis and characterisation

The previously reported preparation of polyIRMOF-1 using ROMP-based poly(pentenamer)s suggested that the poly(octenamer)s prepared here could also form IRMOF-1 structures by applying a similar solvothermal approach.[23] Combining the
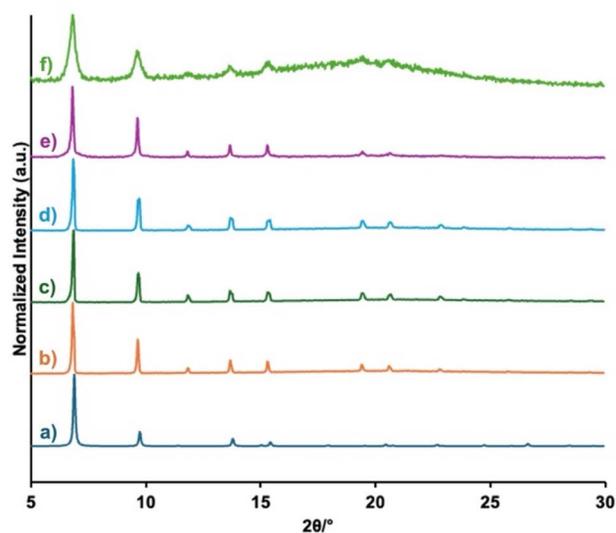

Fig. 3 PXRD pattern of (a) IRMOF-1 (simulated), (b) Zn-poly(OCTbdc-5a)$_{35}$, (c) Zn-*t*Bu-poly(OCTbdc-5a)$_{29}$, (d) Zn-Py-poly(OCTbdc-5a)$_{29}$, (e) Zn-PS$_{12}$-*block*-poly(OCTbdc-5a)$_{23}$-*block*-PS$_{12}$, and (f) Zn-PS$_{30}$-*block*-poly(OCTbdc-5a)$_{23}$-*block*-PS$_{30}$. Approximately 1.5–2 mg of as-synthesized samples were washed with (3 × 1.5 mL) DMF prior to recording their PXRD pattern at room temperature on a Bruker D8 Advance diffractometer with a LynxEye XET detector running at 40 kV, 40 mA for Cu Kα ($\lambda = 1.5418$ Å), with a scan speed of 0.5 s per step, a step size of 0.1° in 2θ, and a 2θ range of 5–30° at room temperature.

polymer ligands with zinc nitrate hexahydrate in DMF at 100 °C for 24 h yielded polyIRMOF-1 materials as pale yellow-to-colourless microcrystalline solids. The polyIRMOF-1 materials were designated as Zn-poly(OCTbdc-5a)$_{35}$ using the homopolymer, Zn-X-poly(OCTbdc-5a)$_{29}$ using amide-capped homopolymers, and Zn-PS$_{0.5m}$-block-poly(OCTbdc-5a)$_{23}$-block-PS$_{0.5m}$ using a triblock copolymer, respectively. PS$_{160}$-block-poly(OCTbdc-5a)$_{23}$-block-PS$_{160}$, with a higher proportion of hydrophobic styrenic blocks, exhibited limited solubility in DMF; as such, no polyMOF material could be synthesised using this block copolymeric linker.

The ATR-FTIR spectrum revealed the characteristic red-shift of the H$_2$bdc carbonyl stretches of poly(OCTbdc-5a)$_{35}$ and PS$_{30}$-block-poly(OCTbdc-5a)$_{23}$-block-PS$_{30}$ upon their conversion to Zn-poly(OCTbdc-5a)$_{35}$ and Zn-PS$_{30}$-block-poly(OCTbdc-5a)$_{23}$-block-PS$_{30}$, respectively, as previously observed with polyMOFs based on poly(pentenamer)s (Fig. S19). Following polyMOF formation, the polymer ligands could be recovered by digesting Zn-poly(OCTbdc-5a)$_{35}$ and Zn-PS$_{30}$-block-poly(OCTbdc-5a)$_{23}$-block-PS$_{30}$, respectively, in a DCl/DMSO mixture. The integrity of the recovered poly(octenamer)s was assessed by ^{1}H NMR spectroscopy, which showed no degradation of the polymers pre- or post-polyMOF formation (Fig. S20).

PXRD analysis of DMF-wetted polyIRMOF-1 materials displayed a pattern consistent with simulated IRMOF-1 (Fig. 3). Zn-poly(OCTbdc-5a)$_{35}$, Zn-X-poly(OCTbdc-5a)$_{29}$, and Zn-PS$_{12}$-block-poly(OCTbdc-5a)$_{23}$-block-PS$_{12}$ exhibited sharp PXRD reflections with a little indication of amorphous phases at 2θ ~20°. Zn-PS$_{30}$-block-poly(OCTbdc-5a)$_{23}$-block-PS$_{30}$ produced a PXRD pattern with reduced crystallinity, as evidenced by the broadness of its corresponding primary reflections (at 2θ ~6.9° and ~9.7°) and greater peak broadness around 2θ ~20°. This is likely due to the lower relative weight fraction (wt%) of the MOF-forming poly(OCTbdc-5a) block with increasing degree of telechelic PS content in PS$_{30}$-block-poly(OCTbdc-5a)$_{23}$-block-PS$_{30}$ (Table S1), as observed with earlier polyMOFs based on block copolymers.[18]

Scanning electron microscopy (SEM) images of Zn-poly(OCTbdc-5a)$_{35}$ and Zn-X-poly(OCTbdc-5a)$_{29}$ showed that these microcrystalline solids exhibited a cubic morphology with irregular sizes and dimensions (Fig. 4a–c). This observation aligns with the characteristics observed in other polyIRMOF-1 materials. In comparison, Zn-PS$_{12}$-block-poly(OCTbdc-5a)$_{23}$-block-PS$_{12}$ particles were spherical aggregates (~0.5–4 µm) of intergrown nanocrystallites (Fig. 4d). Zn-PS$_{30}$-block-poly(OCTbdc-5a)$_{23}$-block-PS$_{30}$ showed an even greater distribution of aggregated nanocrystallites (Fig. 4e). The results indicate that the block copolymer ligands and the length of the terminal blocks significantly influence the morphology of the corresponding polyMOF particles. This is consistent with previous studies on polyMOFs, which have also shown a substantial influence on polymer ligand structure and composition on polyMOF morphology.[18]

The origin of this morphological alteration can be attributed to the extent of accessibility of poly(OCTbdc-5a) chains to the growing IRMOF-1 crystal faces. During the polyMOF growth process, the homopolymer linkers, such as poly(OCTbdc-5a)$_{35}$,
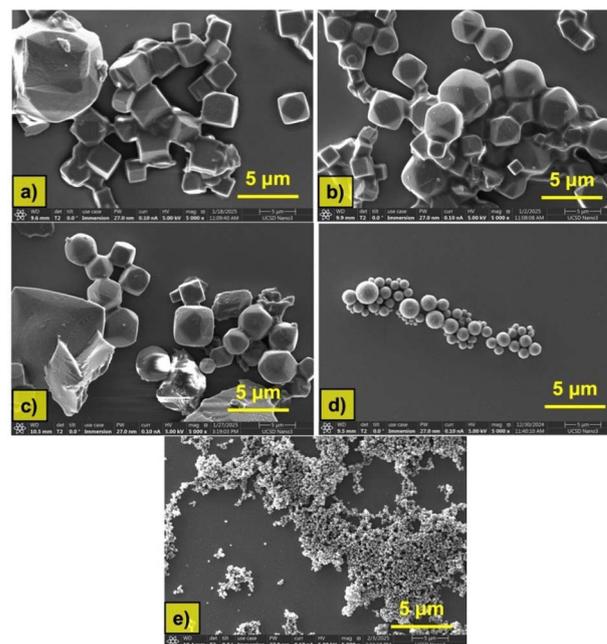

Fig. 4 SEM Images of: (a) Zn-poly(OCTbdc-5a)$_{35}$, (b) Zn-tBu-poly(OCTbdc-5a)$_{29}$, (c) Zn-Py-poly(OCTbdc-5a)$_{29}$, (d) Zn-PS$_{12}$-block-poly(OCTbdc-5a)$_{23}$-block-PS$_{12}$, and (e) Zn-PS$_{30}$-block-poly(OCTbdc-5a)$_{23}$-block-PS$_{30}$.

tBu-poly(OCTbdc-5a)$_{29}$, and Py-poly(OCTbdc-5a)$_{29}$, likely exhibited a better propensity for controlling aggregation, leading to the formation of the corresponding polyMOFs with a cubic morphology. Conversely, the bulky PS domains in the block copolymers likely inhibit the formation of polyMOFs with expected cubic morphology, resulting in the formation of spherical aggregates of nanocrystallites.

Certain MOFs, such as ZIF variants, possess the rare ability to reversibly transform into amorphous, but stable network-forming liquids (melts) or glasses (i.e., exhibit glass transitions) upon heating.[14,36] This results in long-range disordered metal–organic networks with distinct phase behaviours and macroscopic characteristics, making them potentially useful in optics, separation, etc.[20] Inspired by this concept, it was hypothesised that block copolymer ligands could serve as a potential synthetic precursor for obtaining polyMOFs with a discrete non-coordinating amorphous phase that could exhibit glass transition properties. For instance, while the poly(octenamer) block of PS$_{0.5m}$-block-poly(OCTbdc-5a)$_{23}$-block-PS$_{0.5m}$ can promote polyMOF formation, the amorphous PS blocks would remain incapable of forming a polyMOF and rather should display the expected glass transition feature.

To investigate the temperature-dependent behaviour of polyMOFs, poly(OCTbdc-5a)$_{35}$, PS$_{12}$-block-poly(OCTbdc-5a)$_{23}$-block-PS$_{12}$, and PS$_{30}$-block-poly(OCTbdc-5a)$_{23}$-block-PS$_{30}$ were subjected to DSC analysis. The DSC traces of PS$_{12}$-block-poly(OCTbdc-5a)$_{23}$-block-PS$_{12}$ and PS$_{30}$-block-poly(OCTbdc-5a)$_{23}$-block-PS$_{30}$ reveal a distinct T_g attributed to the glass transition of PS block, which is missing in poly(OCTbdc-5a)$_{35}$ (Fig. S21). The PS segments in PS$_{0.5m}$-block-poly(OCTbdc-5a)$_{23}$-block-PS$_{0.5m}$ exhibited a comparable T_g with respect to commercial PS
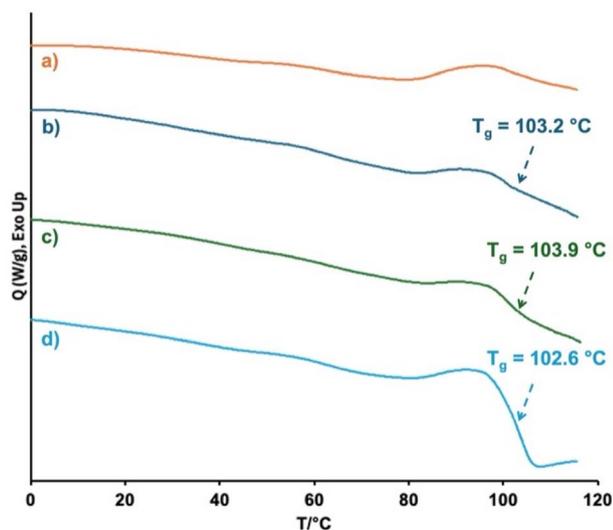
Fig. 5 DSC 2nd heating thermograms of: (a) Zn-poly(OCTbdc-5a)$_{35}$, (b) Zn-PS$_{12}$-block-poly(OCTbdc-5a)$_{23}$-block-PS$_{12}$, (c) Zn-PS$_{30}$-block-poly(OCTbdc-5a)$_{23}$-block-PS$_{30}$, and (d) commercial PS.

(Aldrich, M_w ~280 000; T_g = 102.6 °C). The glass transition behaviour of the poly(octenamer) block was not observed within the measured temperature range (−30 °C to 120 °C). For reference, unfunctionalized poly(octenamer)s generally show T_g close to −80 °C.[37]

Notably, Zn-PS$_{12}$-block-poly(OCTbdc-5a)$_{23}$-block-PS$_{12}$ and Zn-PS$_{30}$-block-poly(OCTbdc-5a)$_{23}$-block-PS$_{30}$ exhibited glass transition behaviour at T_g = 104.5 °C and T_g = 103.6 °C, respectively (Fig. 5). This phenomenon is attributed to the glassy-to-rubbery phase transformation of thermoplastic PS segments within the triblock copolymeric ligand struts of the corresponding polyMOFs, as the transition behaviour exhibited strong similarities to those observed in PS$_{12}$-block-poly(OCTbdc-5a)$_{23}$-block-PS$_{12}$ and PS$_{30}$-block-poly(OCTbdc-5a)$_{23}$-block-PS$_{30}$. This observation suggests that Zn-PS$_{0.5m}$-block-poly(OCTbdc-5a)$_{23}$-block-PS$_{0.5m}$ coexists with distinct phases of polyMOF crystallinity and thermoplastic, amorphous PS domains. The enhanced mobility of discrete PS telechelics enables the corresponding polyMOFs to undergo a rubbery phase transition (at temperatures exceeding the T_g of PS chains), which vitrify during the subsequent cooling cycle (Fig. S21). In contrast, IRMOF-1 (constructed from the molecular H$_2$bdc linker), Zn-poly(OCTbdc-5a)$_{35}$, Zn-tBu-poly(OCTbdc-5a)$_{29}$, and Zn-Py-poly(OCTbdc-5a)$_{29}$ did not exhibit any glass transition characteristics (Fig. 5a and S21).

The heat capacity (C_p) data of the polyMOFs were measured. As expected, the C_p curve of Zn-PS$_{30}$-block-poly(OCTbdc-5a)$_{23}$-block-PS$_{30}$ exhibited a distinct glass transition (Fig. S22). As per the previous reports,[38,39] the onset value (97.1 °C) of this transition is designated as the T_g of Zn-PS$_{30}$-block-poly(OCTbdc-5a)$_{23}$-block-PS$_{30}$, which was found to be comparable with the onset value (98.2 °C) of its glass transition in Fig. 5. More importantly, this glass transition characteristic was absent from the C_p curve of Zn-poly(OCTbdc-5a)$_{35}$. This clearly indicates the

glass transition capability of Zn-PS$_{30}$-block-poly(OCTbdc-5a)$_{23}$-block-PS$_{30}$, whereas Zn-poly(OCTbdc-5a)$_{35}$ lacks this property.

To illustrate the impact of the glass transition feature, the physical forms and structural morphologies of Zn-poly(OCTbdc-5a)$_{35}$ and Zn-PS$_{30}$-block-poly(OCTbdc-5a)$_{23}$-block-PS$_{30}$ were assessed. The temperature used to activate these polyMOF samples (105 °C) is close to the T_g of PS (102.6 °C). As such, the free-flowing powder of Zn-PS$_{30}$-block-poly(OCTbdc-5a)$_{23}$-block-PS$_{30}$ changed to large flakes after heating/activating (Fig. 6b). Some of these flakes exhibited a slightly curved shape, aligning with the concave bottom of the round-bottom flask in which the polyMOF was activated, suggesting their moldability (Fig. S23). SEM imaging of the flakes (Fig. 6d) revealed the coalescence of the nanocrystallites into large, interconnected globular aggregates (compare with the images of the as-synthesised samples in Fig. 4d). This phenomenon is attributed to the glass transition of the PS domains within Zn-PS$_{30}$-block-poly(OCTbdc-5a)$_{23}$-block-PS$_{30}$ that undergo a soft, rubbery phase transition at 105 °C, which facilitates the resulting morphological transformations and "sintering" of the polyMOF nanocrystallites. By contrast, activated Zn-poly(OCTbdc-5a)$_{35}$ was obtained as a solid powder with almost no morphological alterations compared to its pristine form upon activation (Fig. 6a and c). Although the precise reason remains uncertain, the transition of glassy PS chains to a rubbery state during activation of Zn-PS$_{30}$-block-poly(OCTbdc-5a)$_{23}$-block-PS$_{30}$ at 105 °C is likely to have facilitated its morphological transformation. A recent report by Bockstaller et al. reveals the "brush fusion" of PS-grafted silica nanoparticles at a temperature exceeding the glass transition of PS, which resulted in a contiguous film via extensive entanglements of PS brushes.[40] It is plausible that the activation of the polyMOF particles at 105 °C enhanced the "softness" of the PS chains, thereby facilitating the fusion of smaller nanocrystallites through chain entanglements and their conversion to larger, globular aggregates.
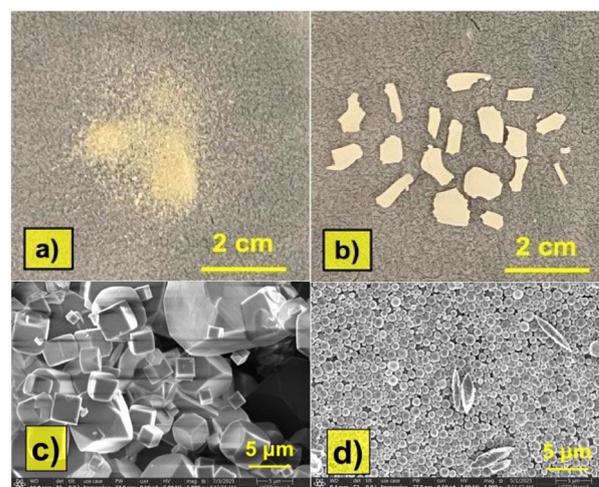

Fig. 6 Photographs of the physical form of: (a) Zn-poly(OCTbdc-5a)$_{35}$ and (b) PS$_{30}$-block-poly(OCTbdc-5a)$_{23}$-block-PS$_{30}$ after activation at 105 °C. SEM images of activated: (c) Zn-poly(OCTbdc-5a)$_{35}$ and (d) Zn-PS$_{30}$-block-poly(OCTbdc-5a)$_{23}$-block-PS$_{30}$.
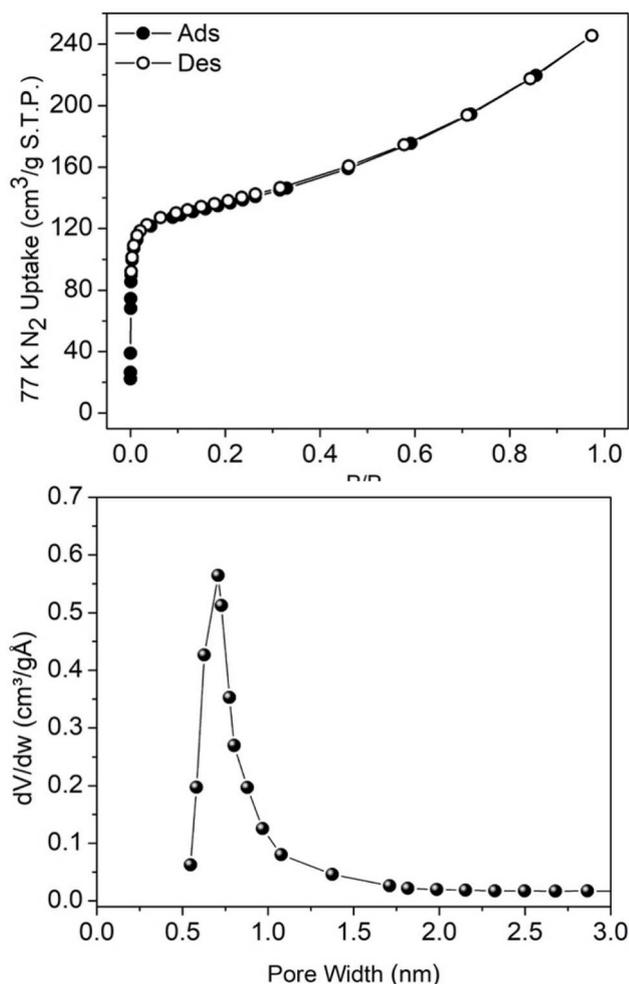
Fig. 7 N$_2$ physisorption isotherm (top) and Horvath–Kawazoe pore width (bottom) plots of Zn-poly(OCTbdc-5a)$_{35}$.

N$_2$ sorption isotherms were carried out on Zn-poly(OCTbdc-5a)$_{35}$, Zn-PS$_{12}$-*block*-poly(OCTbdc-5a)$_{23}$-*block*-PS$_{12}$, and Zn-PS$_{30}$-*block*-poly(OCTbdc-5a)$_{23}$-*block*-PS$_{30}$ at 77 K to investigate their porosity. Zn-poly(OCTbdc-5a)$_{35}$ showed a characteristic type I isotherm dominated by large micropore uptake (Fig. 7). In triplicate experiments, the BET surface area of Zn-poly(OCTbdc-5a)$_{35}$ was found to be 277 ± 119 m^2 g^{-1}. Despite successful initial activation, running a second adsorption–desorption cycle (using the same sample) revealed a total loss of porosity (Fig. S24). This was accompanied by shifts in peak positions and a loss in crystallinity observed in the PXRD pattern of the activated Zn-poly(OCTbdc-5a)$_{35}$ (Fig. S25). Consistent with the large observed error in the BET surface area experiment (277 ± 119 m^2 g^{-1}), the change in the PXRD pattern is attributed to a notable sensitivity of the polyMOF to sample handling conditions[41,42] and the poor adsorptive cycling stability[43–45] of the crystalline framework, resulting in structure collapse.

These sorption experiments show that Zn-poly(OCTbdc-5a)$_{35}$ can exhibit porosity, with a maximum BET surface area of ∼512 m^2 g^{-1} measured. When the mass fraction of the polymer backbone in Zn-poly(OCTbdc-5a)$_{35}$ (which does not contribute

to porosity) is accounted for, an adjusted value of ∼856 m^2 g^{-1} is obtained (Table S2).[46,47] Notably, this value is significantly reduced compared to unmodified IRMOF-1 (3800 m^2 g^{-1}),[41] and as noted above, the observed porosity is not robust. The reduced surface area reflects that a large portion of available pore volume is occupied or blocked by the polymer chains; however, it is regarded as a substantial enhancement when compared to previous generations of polyMOFs based on poly(vinyl ether) or poly(pentenamer)s containing H$_2$bdc pendants.[22,23]

Yazaki *et al.* reported a polyMOF with an IRMOF-1 structure using a homopolymeric poly(vinyl ether) linker with 100% H$_2$bdc incorporation.[22] This polyMOF was non-porous with a BET surface area value of <1 m^2 g^{-1}. The polymeric linker was developed *via* an uncontrolled cationic polymerization method, which limited the ability to control its composition and microstructure. Previously reported IRMOF-1-type polyMOFs using poly(pentenamer)s prepared *via* a controlled ROMP method exhibited porosity, with a BET surface area of ∼500 m^2 g^{-1}. However, the system was limited to random copolymers with only 30% MOF-forming ligand functionalities.[23]

The current system offers a significant improvement compared to both of these prior reports. The utilization of cyclooctene derivatives precisely enabled the formulation of polymeric linkers beyond homopolymer formation and allowed block copolymer synthesis with controlled composition and dispersity. All the linkers were successfully transformed into crystalline, porous polyMOFs resembling the IRMOF-1-type structure. Notably, Zn-poly(OCTbdc-5a)$_{35}$, designed from a homopolymer ligand with 100% H$_2$bdc incorporation as pendants, exhibited accessible porosity.

The micropore volume for Zn-poly(OCTbdc-5a)$_{35}$ was determined to be 0.340 cm^3 g^{-1} at a P/P_0 value of 0.85, with a small contribution from interparticle N$_2$ condensation at higher pressures. The peak pore width for Zn-poly(OCTbdc-5a)$_{35}$ was calculated to be 0.7 nm by the Horvath–Kawazoe method (Fig. 7). Zn-*t*Bu-poly(OCTbdc-5a)$_{29}$ and Zn-Py-poly(OCTbdc-5a)$_{29}$ did not exhibit measurable porosity or BET surface area values (Fig. S26). The isotherms measured with Zn-PS$_{12}$-*block*-poly(OCTbdc-5a)$_{23}$-*block*-PS$_{12}$ and Zn-PS$_{30}$-*block*-poly(OCTbdc-5a)$_{23}$-*block*-PS$_{30}$ showed greatly reduced microporosity, with surface areas of 36 ± 8 m^2 g^{-1} and 10 ± 3 m^2 g^{-1} (Fig. S27), respectively. These correspond to values of 41 m^2 g^{-1} and 96 m^2 g^{-1} after mass adjustment (Table S2), showing that these materials are effectively non-porous. Pore volumes for Zn-PS$_{12}$-*block*-poly(OCTbdc-5a)$_{23}$-*block*-PS$_{12}$ and Zn-PS$_{30}$-*block*-poly(OCTbdc-5a)$_{23}$-*block*-PS$_{30}$ are 0.209 cm^3 g^{-1} and 0.148 cm^3 g^{-1}, respectively, which arise from macropores and are significantly distinct from Zn-poly(OCTbdc-5a)$_{35}$, demonstrating the negligible micropore contribution to uptake compared to Zn-poly(OCTbdc-5a)$_{35}$ (Fig. S28). The peak pore widths for Zn-PS$_{12}$-*block*-poly(OCTbdc-5a)$_{23}$-*block*-PS$_{12}$ and Zn-PS$_{30}$-*block*-poly(OCTbdc-5a)$_{23}$-*block*-PS$_{30}$ are 7.8 Å and 8.1 Å, respectively, but these are associated with significantly lower available volumes (Table S3). The lack of porosity is attributed to the greater polymer-occluded volume in the Zn-PS$_{0.5m}$-*block*-poly(OCTbdc-5a)$_{23}$-*block*-PS$_{0.5m}$ materials, as well as a tendency towards loss of crystallinity or pore collapse. PXRD shows that the primary reflections at 2θ ∼6.8° and ∼9.6°

were broadened and slightly shifted to higher angles (2θ of $\sim 7.2°$ and $\sim 9.9°$, respectively) following the activation of Zn-PS$_{30}$-*block*-poly(OCTbdc-5a)$_{23}$-*block*-PS$_{30}$ at either 40 °C (24 h) or 105 °C (10 h, Fig. S25). A comparable shift was also observed in earlier polyIRMOF-1 materials composed of styrenic block copolymeric linkers containing ligand units (H$_2$bdc) in their backbone, suggesting the general instability of these polyMOFs under the activated (solvent-free) conditions.[17]

To clarify if activating the polyMOFs at 105 °C has any influence on their crystallinity or porosity, the N$_2$ gas sorption experiment was additionally performed by activating Zn-poly(-OCTbdc-5a)$_{35}$ at 50 °C for 24 h. However, the measured BET surface area value (~ 83 m^2 g^{-1}) was found to be significantly lower than the best value recorded after activating the sample at 105 °C for 10 h (~ 512 m^2 g^{-1}, Fig. S29). This observation suggests that lowering the activation temperature does not improve the polyMOF porosity.

In addition, the ambient stability of the polyMOFs was assessed by recording the PXRD patterns of DMF-wetted Zn-poly(OCTbdc-5a)$_{35}$ and Zn-PS$_{30}$-*block*-poly(OCTbdc-5a)$_{23}$-*block*-PS$_{30}$ after storage under ambient conditions for 1 day and 1 week, respectively. After 1 day, Zn-poly(OCTbdc-5a)$_{35}$ retained crystallinity, however, with a notable shift in reflections at 2θ $\sim 6.8°$ and $\sim 9.7°$ to ~ 7.2 and ~ 10.2, respectively (Fig. S30). By contrast, the PXRD pattern of Zn-PS$_{30}$-*block*-poly(OCTbdc-5a)$_{23}$-*block*-PS$_{30}$ showed a pronounced loss in crystallinity with missing and broadened peaks (in addition to a similar shift in 2θ of $\sim 6.8°$ to 7.4°). The PXRD patterns for both materials obtained after 1 day of aging remained essentially unchanged after 1 week of aging under ambient conditions.

The results are consistent with previous polyMOF systems constructed from poly(pentamer)s,[23] where monitoring *via* PXRD also showed substantial peak broadening after ambient storage for 1 day or 1 week (although these systems showed smaller peak shifts and reductions in peak intensity). This suggests that different polyMOF systems (*i.e.*, poly(pentamer)s *vs.* poly(octenamer)s) do not show particularly pronounced differences in stability in these somewhat related systems. This observation further implies that the activation of the samples has no substantial impact on the polyMOF crystallinity or porosity, and the pore collapse likely occurs due to the propensity of poly(octenamer)-based polyMOFs to undergo distinct phase transformation into an unidentified crystalline phase during their storage under ambient conditions or even at room temperature in an air-free environment.

However, the original crystallinity of such activated poly-MOFs can be restored by re-exposing the materials to DMF.[4,17] Activated Zn-poly(OCTbdc-5a)$_{35}$ and Zn-PS$_{30}$-*block*-poly(-OCTbdc-5a)$_{23}$-*block*-PS$_{30}$ powder samples were heated in DMF for 1 h at 60 °C resulting in complete restoration of crystallinity as determined by the PXRD analysis (Fig. S31).

Conclusions

In summary, this work represents a significant advancement in the synthesis and understanding of polyMOFs. Earlier reported methodologies for preparing polymer ligands exhibited substantial limitations in terms of control over polymer architecture with a lack of control over molecular weights, and an inability to incorporate active sites for end-coupling functionalization. Herein, accessing symmetric CTA-mediated ROMP, the homopolymeric poly(OCTbdc-5e) was synthesised with a suitable pentafluorophenyl ester and RAFT telechelics. The reactive termini enabled the poly(OCTbdc-5e) constructs to be functionalized with amines and thermoplastic PS chains that were successfully transformed into polyIRMOF-1 structures. The distinct PS blocks enabled the corresponding polyMOFs to exhibit glass transition behaviour at approximately 105 °C, while simultaneously retaining a degree of IRMOF crystallinity. RAFT telechelics should present a multitude of opportunities to install various functional vinyl (macro)monomers, including macromolecular brushes.[48] Accessing such tailor-made, tandem polymerisation approaches would potentially unravel unique thermal, structural, as well as morphological properties within the context of polyMOFs. Moreover, given that these polyMOFs exhibit glass transition, which facilitate their processing into sub-continuous flakes while maintaining accessible pores, such materials could find applications as membranes in relevant domains.

Author contributions

The manuscript was written through the contributions of all authors. All authors have given approval to the final version of the manuscript. P. M. and S. M. C. designed the materials and experimental strategy; P. M. conducted the experiments; D. S. evaluated the gas sorption behaviour of the materials; P. M. and D. S. wrote the manuscript; P. M. and S. M. C. supervised the editing of the manuscript. All authors have given approval to the final version of the manuscript.

Conflicts of interest

There are no conflicts to declare.

Data availability

The data supporting this article have been included as part of the supplementary information (SI). The raw experimental data are saved in a custom format and will be shared upon request. Supplementary information: it describes the detailed experimental and characterization procedures for all reported studies. See DOI: **https://doi.org/10.1039/d5sc05704c**.

Acknowledgements

Notes and references

1 D. J. Tranchemontagne, J. L. Mendoza-Cortés, M. O'Keeffe and O. M. Yaghi, Secondary building units, nets and bonding in the chemistry of metal–organic frameworks, *Chem. Soc. Rev.*, 2009, **38**, 1257–1283.

2 T. Kitao, Y. Zhang, S. Kitagawa, B. Wang and T. Uemura, Hybridization of MOFs and polymers, *Chem. Soc. Rev.*, 2017, **46**, 3108–3133.

3 M. Kalaj, K. C. Bentz, S. Ayala Jr, J. M. Palomba, K. S. Barcus, Y. Katayama and S. M. Cohen, MOF-Polymer Hybrid Materials: From Simple Composites to Tailored Architectures, *Chem. Rev.*, 2020, **120**, 8267–8302.

4 Z. Zhang, H. T. H. Nguyen, S. A. Miller and S. M. Cohen, polyMOFs: A Class of Interconvertible Polymer-Metal-Organic-Framework Hybrid Materials, *Angew. Chem. Int. Ed.*, 2015, **54**, 6152–6157.

5 M. A. Pearson, M. Dincă and J. A. Johnson, Radical PolyMOFs: A Role for Ligand Dispersity in Enabling Crystallinity, *Chem. Mater.*, 2021, **33**, 9508–9514.

6 T. Hyun, J. Park, J. So, J. Kim and D.-Y. Koh, Unexpected Molecular Sieving of Xylene Isomer Using Tethered Ligand in Polymer-Metal–Organic Frameworks (polyMOFs), *Adv. Sci.*, 2024, **11**, 2402980.

7 Z. Zhang, H. T. H. Nguyen, S. A. Miller, A. M. Ploskonka, J. B. DeCoste and S. M. Cohen, Polymer–Metal–Organic Frameworks (polyMOFs) as Water Tolerant Materials for Selective Carbon Dioxide Separations, *J. Am. Chem. Soc.*, 2016, **138**, 920–925.

8 P. G. M. Mileo, S. Yuan, S. Ayala Jr, P. Duan, R. Semino, S. M. Cohen, K. Schmidt-Rohr and G. Maurin, Structure of the Polymer Backbones in polyMOF Materials, *J. Am. Chem. Soc.*, 2020, **142**, 10863–10868.

9 K. Suresh, C. A. Carey and A. J. Matzger, Metal–Organic Frameworks (MOFs) Morphology Control: Recent Progress and Challenges, *Cryst. Growth Des.*, 2024, **24**, 2288–2300.

10 C. V. McGuire and R. S. Forgan, The surface chemistry of metal–organic frameworks, *Chem. Commun.*, 2015, **51**, 5199–5217.

11 C. Pathak, S. Mistry and S. Seth, Morphological variation of metal-organic frameworks and its impacts on their functional properties, *Coord. Chem. Rev.*, 2025, **543**, 216928.

12 J. Łuczak, M. Kroczewska, M. Baluk, J. Sowik, P. Mazierski and A. Zaleska-Medynska, Morphology control through the synthesis of metal-organic frameworks, *Adv. Colloid. Interface Sci*, 2023, **314**, 102864.

13 M. Liu, L. Zu and Z. M. Hudson, Mechanistic Principles for Engineering Hierarchical Porous Metal–Organic Frameworks, *ACS Nano*, 2022, **16**, 13573–13594.

14 N. Ma and S. Horike, Metal–Organic Network-Forming Glasses, *Chem. Rev.*, 2022, **122**, 4163–4203.

15 C. Healy, K. M. Patil, B. H. Wilson, L. Hermanspahn, N. C. Harvey-Reid, B. I. Howard, C. Kleinjan, J. Kolien, F. Payet, S. G. Telfer, P. E. Kruger and T. D. Bennett, The thermal stability of metal-organic frameworks, *Coord. Chem. Rev.*, 2020, **419**, 213388.

16 T. D. Bennett, S. Horike, J. C. Mauro, M. M. Smedskjaer and L. Wondraczek, Looking into the future of hybrid glasses, *Nat. Chem.*, 2024, **16**, 1755–1766.

17 M. J. MacLeod and J. A. Johnson, Block co-polyMOFs: assembly of polymer–polyMOF hybrids via iterative exponential growth and "click" chemistry, *Polym. Chem.*, 2017, **8**, 4488–4493.

18 S. Ayala, K. C. Bentz and S. M. Cohen, Block co-polyMOFs: morphology control of polymer–MOF hybrid materials, *Chem. Sci.*, 2019, **10**, 1746–1753.

19 K. C. Bentz, K. Gnanasekaran, J. B. Bailey, S. Ayala, F. A. Tezcan, N. C. Gianneschi and S. M. Cohen, Inside polyMOFs: layered structures in polymer-based metal–organic frameworks, *Chem. Sci.*, 2020, **11**, 10523–10528.

20 M. Liu, A. H. Slavney, S. Tao, R. D. McGillicuddy, C. C. Lee, M. B. Wenny, S. J. L. Billinge and J. A. Mason, Designing Glass and Crystalline Phases of Metal–Bis(acetamide) Networks to Promote High Optical Contrast, *J. Am. Chem. Soc.*, 2022, **144**, 22262–22271.

21 M. Kim, H.-S. Lee, D.-H. Seo, S. J. Cho, E.-c. Jeon and H. R. Moon, Melt-quenched carboxylate metal–organic framework glasses, *Nat. Commun.*, 2024, **15**, 1174.

22 K. Yazaki, M. Takahashi, N. Miyajima and M. Obata, Construction of a polyMOF using a polymer ligand bearing the benzenedicarboxylic acid moiety in the side chain, *New J. Chem.*, 2020, **44**, 5182–5185.

23 P. Mondal, D. Sensharma and S. M. Cohen, Polymer–Metal–Organic Frameworks (polyMOFs) Based on Tailor-Made Poly(alkenamer)s, *Chem. Mater.*, 2024, **36**, 9696–9703.

24 K. Horie, M. Barón, R. B. Fox, J. He, M. Hess, J. Kahovec, T. Kitayama, P. Kubisa, E. Maréchal, W. Mormann, R. F. T. Stepto, D. Tabak, J. Vohlídal, E. S. Wilks and W. J. Work, Definitions of terms relating to reactions of polymers and to functional polymeric materials (IUPAC Recommendations 2003), *Pure Appl. Chem.*, 2004, **76**, 889–906.

25 H. Martinez and M. A. Hillmyer, Carboxy-Telechelic Polyolefins in Cross-Linked Elastomers, *Macromolecules*, 2014, **47**, 479–485.

26 C. S. Sample, E. A. Kellstedt and M. A. Hillmyer, Tandem ROMP/Hydrogenation Approach to Hydroxy-Telechelic Linear Polyethylene, *ACS Macro Lett.*, 2022, **11**, 608–614.

27 A. K. Diallo, L. Annunziata, S. Fouquay, G. Michaud, F. Simon, J.-M. Brusson, S. M. Guillaume and J.-F. Carpentier, Ring-opening metathesis polymerization of cyclooctene derivatives with chain transfer agents

derived from glycerol carbonate, *Polym. Chem.*, 2014, **5**, 2583–2591.

28 H. Martinez, N. Ren, M. E. Matta and M. A. Hillmyer, Ring-opening metathesis polymerization of 8-membered cyclic olefins, *Polym. Chem.*, 2014, **5**, 3507–3532.

29 A. R. Hlil, J. Balogh, S. Moncho, H.-L. Su, R. Tuba, E. N. Brothers, M. Al-Hashimi and H. S. Bazzi, Ring opening metathesis polymerization (ROMP) of five- to eight-membered cyclic olefins: Computational, thermodynamic, and experimental approach, *J. Polym. Sci. Part A: Polym. Chem.*, 2017, **55**, 3137–3145.

30 J. B. Matson and R. H. Grubbs, Monotelechelic Poly(oxa) norbornenes by Ring-Opening Metathesis Polymerization Using Direct End-Capping and Cross-Metathesis, *Macromolecules*, 2010, **43**, 213–221.

31 J. B. Matson and R. H. Grubbs, ROMP−ATRP Block Copolymers Prepared from Monotelechelic Poly(oxa) norbornenes Using a Difunctional Terminating Agent, *Macromolecules*, 2008, **41**, 5626–5631.

32 R. Revanur, B. McCloskey, K. Breitenkamp, B. D. Freeman and T. Emrick, Reactive Amphiphilic Graft Copolymer Coatings Applied to Poly(vinylidene fluoride) Ultrafiltration Membranes, *Macromolecules*, 2007, **40**, 3624–3630.

33 A. E. Madkour, A. H. R. Koch, K. Lienkamp and G. N. Tew, End-Functionalized ROMP Polymers for Biomedical Applications, *Macromolecules*, 2010, **43**, 4557–4561.

34 T. Morita, B. R. Maughon, C. W. Bielawski and R. H. Grubbs, A Ring-Opening Metathesis Polymerization (ROMP) Approach to Carboxyl- and Amino-Terminated Telechelic Poly(butadiene)s, *Macromolecules*, 2000, **33**, 6621–6623.

35 M. K. Mahanthappa, F. S. Bates and M. A. Hillmyer, Synthesis of ABA Triblock Copolymers by a Tandem ROMP−RAFT Strategy, *Macromolecules*, 2005, **38**, 7890–7894.

36 T. D. Bennett, S. Horike, J. C. Mauro, M. M. Smedskjaer and L. Wondraczek, Looking into the future of hybrid glasses, *Nat. Chem.*, 2024, **16**, 1755–1766.

37 L. M. Pitet, J. Zhang and M. A. Hillmyer, Sequential ROMP of cyclooctenes as a route to linear polyethylene block copolymers, *Dalton Trans.*, 2013, **42**, 9079–9088.

38 O. Smirnova, S. Hwang, R. Sajzew, L. Ge, A. Reupert, V. Nozari, S. Savani, C. Chmelik, M. R. Reithofer, L. Wondraczek, J. Kärger and A. Knebel, Precise control

over gas-transporting channels in zeolitic imidazolate framework glasses, *Nat. Mater.*, 2024, **23**, 262–270.

39 V. Nozari, O. Smirnova, J. M. Tuffnell, A. Knebel, T. D. Bennett and L. Wondraczek, Low-Temperature Melting and Glass Formation of the Zeolitic Imidazolate Frameworks ZIF-62 and ZIF-76 through Ionic Liquid Incorporation, *Adv. Mater. Technol.*, 2022, **7**, 2200343.

40 Y. Cang, A. N. Reuss, J. Lee, J. Yan, J. Zhang, E. Alonso-Redondo, R. Sainidou, P. Rembert, K. Matyjaszewski, M. R. Bockstaller and G. Fytas, Thermomechanical Properties and Glass Dynamics of Polymer-Tethered Colloidal Particles and Films, *Macromolecules*, 2017, **50**, 8658–8669.

41 S. S. Kaye, A. Dailly, O. M. Yaghi and J. R. Long, Impact of Preparation and Handling on the Hydrogen Storage Properties of $Zn_4O(1,4-benzenedicarboxylate)_3$ (MOF-5), *J. Am. Chem. Soc.*, 2007, **129**, 14176–14177.

42 Y. Ming, J. Purewal, J. Yang, C. Xu, R. Soltis, J. Warner, M. Veenstra, M. Gaab, U. Müller and D. J. Siegel, Kinetic Stability of MOF-5 in Humid Environments: Impact of Powder Densification, Humidity Level, and Exposure Time, *Langmuir*, 2015, **31**, 4988–4995.

43 J. T. Hughes and A. Navrotsky, MOF-5: Enthalpy of Formation and Energy Landscape of Porous Materials, *J. Am. Chem. Soc.*, 2011, **133**, 9184–9187.

44 M. Ding, X. Cai and H.-L. Jiang, Improving MOF stability: approaches and applications, *Chem. Sci.*, 2019, **10**, 10209–10230.

45 X. Liu, Y. Li, Y. Ban, Y. Peng, H. Jin, H. Bux, L. Xu, J. Caro and W. Yang, Improvement of hydrothermal stability of zeolitic imidazolate frameworks, *Chem. Commun.*, 2013, **49**, 9140–9142.

46 V. J. Pastore, T. R. Cook and J. Rzayev, Polymer–MOF Hybrid Composites with High Porosity and Stability through Surface-Selective Ligand Exchange, *Chem. Mater.*, 2018, **30**, 8639–8649.

47 M. A. Pearson, S. Bhagchandani, M. Dincă and J. A. Johnson, Mixing ligands to enhance gas uptake in polyMOFs, *Mol. Syst. Des. Eng.*, 2023, **8**, 591–597.

48 S. Perrier, 50th Anniversary Perspective: RAFT Polymerization—A User Guide, *Macromolecules*, 2017, **50**, 7433–7447.